Development of a Continuous, Uncoupled Fluorescence-based Assay for Monitoring Methyltransferase Activity: Methylation Going Sour

Benjamin Panagiotis Chapple, Lisa M. Böhmer, Jörg Pietruszka

ChemCatChem

ChemCatChem
Chemistry Europe
European Chemical Societies Publishing

RESEARCH ARTICLE OPEN ACCESS

Development of a Continuous, Uncoupled Fluorescence-based Assay for Monitoring Methyltransferase Activity: *Methylation Going Sour*

Benjamin Panagiotis Chapple[1,+] | Lisa M. Böhmer[1,+] | Jörg Pietruszka[1,2]

[1]Institute For Bioorganic Chemistry & Bioeconomy Science Center (BioSC), Heinrich Heine University Düsseldorf in Forschungszentrum Jülich, Jülich, Germany | [2]Institute of Bio- and Geosciences (IBG-1: Bioorganic Chemistry), Forschungszentrum Jülich, Jülich, Germany

Correspondence: Jörg Pietruszka (j.pietruszka@fz-juelich.de)

Received: 10 November 2025 | **Revised:** 15 January 2026 | **Accepted:** 18 January 2026

Keywords: enzyme assay | fluorescent probes | high-throughput screening | methyltransferase | natural products

ABSTRACT

Methyltransferases (MTs) are versatile biocatalysts capable of regio-, stereo-, and enantioselective methylation of molecules, making them particularly valuable for late-stage functionalization of natural products and their analogues. To further broaden the applicability of these enzymes, it is essential to gain knowledge about their mode of catalysis and develop effective enzyme engineering and screening strategies. This, in turn, requires the development and application of robust analytical techniques, especially when dealing with large-scale screenings, such as those involved in mutagenesis campaigns. In this study, we have established the first uncoupled, continuous, fluorescence-based, high-throughput assay that serves as a close-to-universal system for activity determination of *S*-adenosyl-L-methionine-dependent MTs. The assay is based on proton release during the methylation, and its use is not limited to purified enzymes, but can also be applied with cell-free extracts and, in certain cases, pre-treated whole cells. To validate its applicability, activities of three distinct MTs with different substrate acceptor atoms (*C*, *N*, and *O*) were determined, and the results were benchmarked against HPLC analysis. Additionally, the assay's utility was demonstrated through a substrate scope screening and the determination of kinetic parameters. Finally, the Z'-factor was evaluated for two different potential enzyme setups to assess the assay's suitability for high-throughput applications.

1 | Introduction

Methylation is a fundamental biochemical process found across all domains of life, ranging from DNA and RNA methylation, which are central to epigenetic regulation and gene expression, to the diversification of natural products. In the context of synthetic chemistry and the development of active pharmaceutical ingredients, methylation can be a valuable tool for late-stage functionalization [1, 2]. The so-called 'magic methyl effect' describes how the introduction of a single methyl group can drastically improve a compound's potency, selectivity, or pharmacokinetic profile by modulating its biochemical properties [3]. However, achieving selective methylation, especially in the final stages of complex molecule synthesis, remains a significant challenge in organic chemistry [4]. Chemical methylation often requires toxic alkylating agents and harsh, environmentally unfriendly reaction conditions [5]. The presence of multiple nucleophilic sites within a molecule often necessitates the use of protecting groups, a complete redesign of synthetic routes to enable early-stage methylation, or the use of pre-methylated building blocks [6].

[+]Benjamin Panagiotis Chapple and Lisa M. Böhmer have contributed equally to this work.

S-Adenosyl-L-methionine (SAM)-dependent methyltransferases (MTs) offer an attractive biocatalytic alternative, providing high levels of chemo-, regio-, and stereoselectivity under mild reaction conditions. These enzymes are capable of methylating heteroatoms as well as carbon centers and have been successfully applied in the (chemo)enzymatic synthesis of diverse target molecules [7]. Advances in MT enzyme engineering, substrate scope expansion, SAM analogue utilization, and cofactor regeneration have significantly improved the accessibility and practicability of MTs as biocatalysts [8–12]. While considerable progress has been achieved in the field, identifying and engineering novel MT variants continues to present difficulties, in part due to the limited availability of robust, high-throughput-compatible activity assays, particularly those suitable for use with nonpurified catalysts.

Classical endpoint methods based on HPLC or GC remain the gold standard for quantification of MT activity, but are time-consuming and low-throughput [13]. Other direct methods employ radioactive probes, but their handling complexity and safety requirements limit their applicability in most laboratory settings [14]. In addition, assay systems tailored to specific substrate classes have been established, though their high degree of specificity serves as both a benefit and a constraint [15, 16]. To address these limitations, a variety of general MT activity detection assays have been developed over the past two decades, all being enzyme-coupled. Most methods rely on the indirect detection of MT activity by linking the formation of *S*-adenosyl-L-homocysteine (SAH), the stoichiometric by-product of SAM-dependent methylation, to downstream enzymatic cascades that generate a measurable photometric or fluorescent signal (Figure 1). Many of these assays fall into two mechanistic classes: NADH/NAD^+-based dehydrogenase-coupled systems, and thiol- or sulfide-detection assays. The first strategy relies on NADH depletion, where SAH is enzymatically degraded to intermediates that release ammonia or adenosine, which in turn are processed in a coupled enzymatic reaction to oxidize NADH to NAD^+. For example, the assay by Simon-Baram et al. employs SAH deaminase to generate ammonia, which is converted to glutamate by glutamate dehydrogenase, depleting NADH and decreasing absorbance at 340 nm, overall simplifying earlier work by Duchin et al. by reducing the number of enzymes needed for the generation of ammonia [17, 18]. Similarly, Kailing et al. used a four-step enzymatic detection cascade, starting with SAH hydrolase and ending with lactate dehydrogenase to achieve NADH consumption through a parallel route *via* adenosine conversion [19]. While sensitive, these approaches might suffer from high background due to endogenous NADH-dependent enzymes when used with nonpurified catalyst formulations. In contrast, the second strategy relies on thiol-detection, leveraging SAH hydrolysis to homocysteine, which is quantified using reagents like *Ellman*'s reagent or monobromobimane [20, 21]. However, their lack of selectivity when reacting with cellular thiols such as glutathione limits their use with cell-free extracts (CFEs). To overcome this limitation and address the discontinuous nature of these systems, more selective detection routes based on homocysteine conversion to H_2S have been designed. These couple homocysteine α,γ-lyase to sulfide-

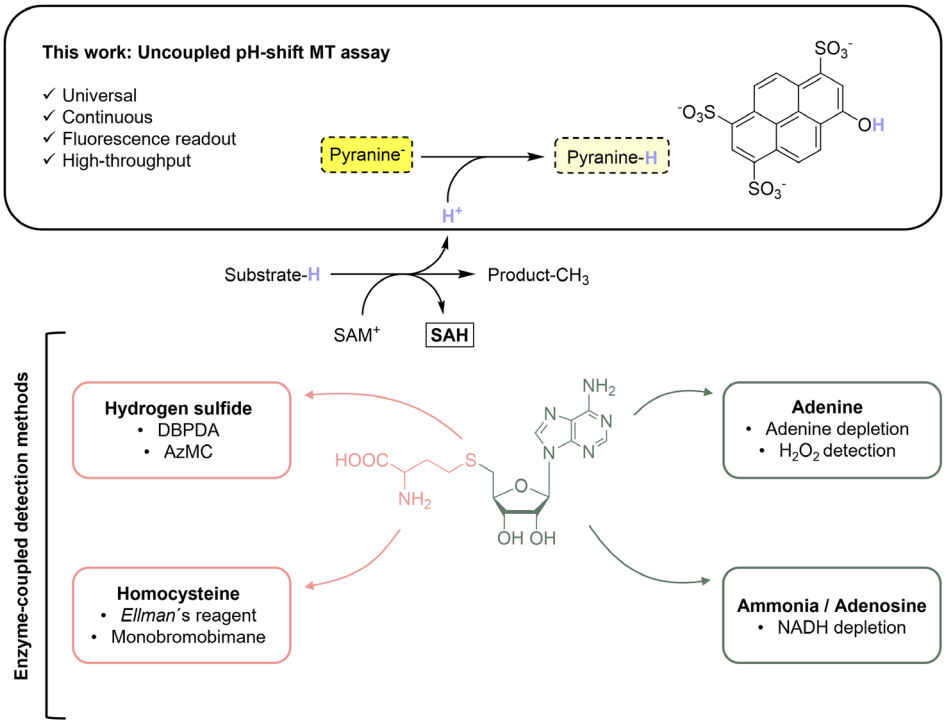

FIGURE 1 | Overview of different enzyme-coupled detection systems for MT activity determination, as well as the uncoupled assay system described in this work. Enzyme-coupled assays are based on SAH formation during the methylation reaction and subsequent conversion of this molecule into a detectable photometric or fluorescent output *via* enzymatic cascades. These assays may detect a readout based on adenine depletion or conversion [24, 25], NADH depletion and detection through ammonia/adenosine conversion [17, 19], homocysteine-coupled detection [20, 21], or hydrogen sulfide-coupled detection [22, 23]. The uncoupled assay described in this work relies on protons released during the MT-catalyzed reaction, which are detected using the fluorescent pH-indicator pyranine (***1***). This ultimately results in a decrease in fluorescence. For additional details, see the main text.

responsive fluorophores such as *N*,*N*-dibutyl phenylene diamine (DBPDA) in the work of Tan et al., or 7-azido-4-methylcoumarin (AzMC) as shown by Menke et al., the latter enabling real-time fluorescence monitoring using CFEs and reducing background by targeting specifically H_2S rather than thiol presence directly [22, 23]. Beyond the NADH- and thiol-/sulfur-based methods, two other notable continuous enzyme-based assays utilize alternative detection chemistries. Akhtar et al. constructed an enzymatic cascade to generate H_2O_2 starting from SAH, which can be quantified using the commercially available but expensive reagent Amplex Red, producing the measurable fluorogenic oxidation product resorufin [24]. Alternatively, Dorgan et al. designed a two-step enzymatic cascade that converts SAH to adenine and subsequently to hypoxanthine, resulting in a measurable decrease in UV absorbance at 265 nm [25]. However, this method can suffer from relatively low sensitivity due to high background absorbance from other biomolecules, such as nucleic acids.

Since SAH can also inhibit SAM-dependent MTs, assay systems based on the depletion of SAH can serve two purposes [26]. However, current systems have the disadvantage of requiring up to five different (purified) enzymes for detection, and most of them only working with purified catalysts, as in the case of the discontinuous and commercially available MTase-Glo assay [27]. The enzyme-coupled nature of these assays introduces variability and increases complexity and cost, which also limits their applicability, particularly in high-throughput screenings, and especially if they can only be applied using purified MTs. Depending on the required screening accuracy, uncoupled assays that rely solely on a small-molecule reporter could be a convenient alternative. pH-Shift assays are a promising class of such uncoupled systems is, which detect changes in proton concentration resulting from enzymatic activity [28]. These assays typically employ colorimetric pH indicators and have been successfully applied to monitor the activity of a range of proton releasing enzymatical reactions, including dehalogenases, decarboxylases, esterases, and various transferases [29–32].

This study builds upon previous research involving pH-shift enzyme activity assays [32, 33], establishing the first continuous, uncoupled, and fluorescence-based assay for SAM-dependent methyltransferases. Since the assay directly monitors the release of protons during methylation, it is applicable to all proton-releasing MT-catalyzed reactions (i.e., MTs that methylate thioethers [34] cannot be monitored) and thus obviates the need for any additional enzymes for detection. The applicability of the assay was validated across different methyltransferases (*C*-, *O*-, and *N*-MTs) and catalyst formulations, including purified enzymes, CFEs, and whole-cell systems. Furthermore, for selected enzymes, a substrate scope was screened, and kinetic parameters were determined. Lastly, the Z'-factor was determined to evaluate the potential of the assay for high-throughput applications, such as MT mutagenesis campaigns. Experimental results were benchmarked against HPLC analysis for validation, and differences between both measurement techniques were quantified through the determination of the recovery rate. This work aims to complement existing methods by providing a cost-effective, uncoupled, high-throughput alternative to assess the activity of methyltransferases.

2 | Results and Discussion

2.1 | Choice of Fluorophore

Many enzymatic reactions release or consume protons, leading to a measurable pH-shift. Most SAM-dependent MT catalyzed reactions fall into this scheme, releasing one proton after the catalyzed nucleophilic substitution, leading to the methylated product. Fluorescence-based indicators offer the advantage of providing higher sensitivity than absorbance-based indicators, leading to a wider dynamic range and lower background, especially when used with CFEs and whole-cell systems [35].

For this study, pyranine (8-hydroxypyrene-1,3,6-trisulfonic acid) (***1***) was chosen as the pH indicator as it has the advantages of showing high fluorescence, photostability, and water-solubility as well as being inexpensive and nontoxic [36]. Furthermore, it has been widely used in cell microscopy and fluorescence imaging, and, more recently, in activity assays for dehalogenases and other enzyme classes [32, 33]. One major advantage of this dye is its use for ratiometric measurement, which allows for intrinsic signal normalization and minimizes interference from variables like fluctuations in excitation intensity or indicator concentration [37].

The spectroscopic properties of pyranine were investigated with respect to previously reported characterizations [32, 33]. The flu-

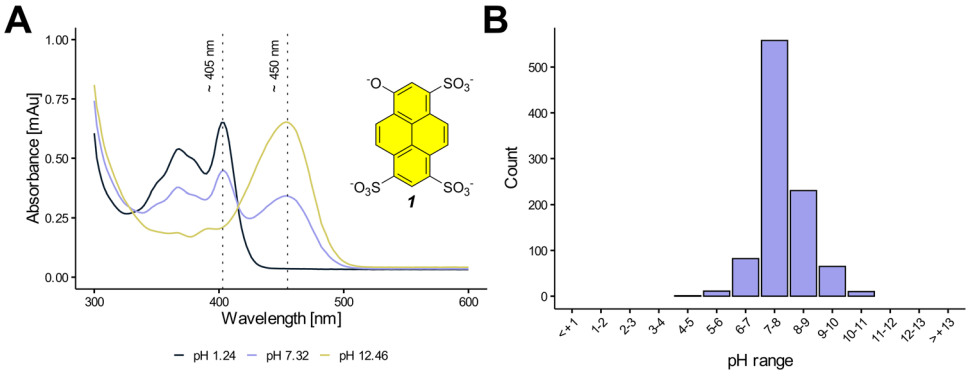

FIGURE 2 | (A) Absorbance spectra of pyranine (***1***) measured in the range of 300–600 nm, showing pH-dependent maxima at 405 nm and 450 nm. (B) Depiction of the pH optima of methyltransferases (EC 2.1.1.-) according to data from the BRENDA database [38].

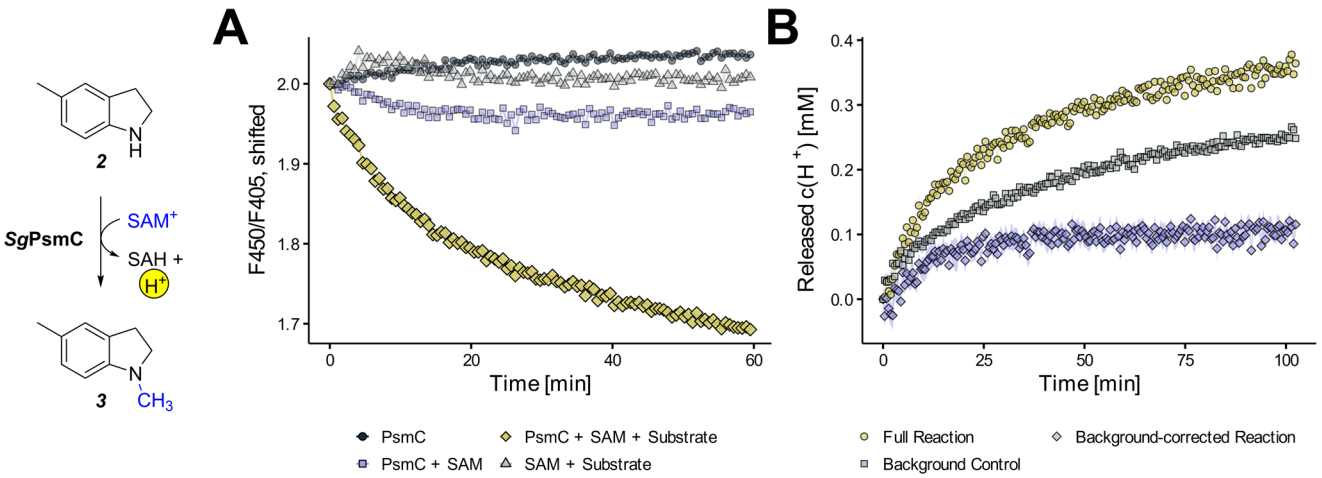

FIGURE 3 | Results of a series of experiments investigating the use of the assay for initial measurement of the *Sg*PsmC-catalyzed *N*-methylation of 5-methyl indoline (***2***) (left). (A) The initial measurement of the reaction (diamonds) is depicted as a decrease in fluorescence (F450/F405) over time. The reaction mixture contained 20 μM of enzyme, 1 mM of 5-methyl indoline (***2***), 2 mM SAM, and 50 μM pyranine in 1 mM potassium phosphate buffer (pH 7.5) at 35 °C. For comparison, negative controls were prepared by omitting individual reaction components. Fluorescence ratio shifted to a common intercept for visual aid. (B) Released c(H^+) during the *Sg*PsmC-catalyzed reaction ('Full Reaction') was measured using 5 μM of enzyme, 1 mM of SAM, 1 mM of 5-methyl indoline (***2***), and 50 μM pyranine in 3 mM sodium phosphate buffer (pH 7.5) at 35 °C. The background control was prepared without an enzyme. For the background-corrected data, the background control was subtracted from the full reaction. c(H^+) was calculated from the F450/F405 ratio using the respective calibration curve.

orophore exhibits a distinct pH-dependent absorbance behavior, which is the basis for the ratiometric measurement (Figure 2A). The fluorescence emission of pyranine is largely pH-independent, with a maximum at approximately 510 nm (see Figure S2). The large *Stokes* shift minimizes self-absorption and results in a clearer signal with reduced background interference. Importantly, the excitation and emission wavelengths of pyranine are compatible with common filter sets used in fluorescence plate readers, and they neither overlap with the absorbance spectra of the substrates used in this study (see Figure S3) nor the intrinsic absorbance of polystyrene-based commercially available microtiter plates, which predominantly absorb around 280 nm.

The apparent pK_a value of pyranine was determined to be 7.36 (see Figure S4) using potassium phosphate buffer across a defined pH range at an indicator concentration of 50 μM and 25 °C. This value is consistent with previously reported ones [33]. Pyranine shows sensitivity in the range of approximately pH 6–8, and the apparent pK_a defines the operational range for the assay, which aligns well with the conditions of most MT-catalyzed reactions, typically showing pH optima in the range of pH 7–8 according to data from the BRENDA database (Figure 2B) [38].

2.2 | Initial Measurement of MT Activity

To assess the applicability of a pyranine-based fluorescent pH-shift assay, the *N*-methyltransferase *Sg*PsmC from *Streptomyces griseofuscus* was selected as a model enzyme for the methylation of 5-methyl indoline (***2***) as an initial proof-of-concept reaction [39, 40].

Different reaction setups were used, including the complete reaction containing all components (*Sg*PsmC, 5-methyl indoline, SAM, and pyranine) and negative controls lacking individual reaction components. The ratio of the fluorescence signal after excitation at 450 nm and 405 nm (F450/F405) was monitored over one hour for both the enzymatic reaction and the negative controls (Figure 3A). The results revealed a substantial decrease for F450/F405 over time exclusively for the enzymatic reaction, indicating that MT activity can indeed be monitored by observing the pH-shift stemming from the acidification of the solution upon proton release.

To quantify the proton release based on the fluorescence signal, a calibration of F450/F405 versus defined concentrations of H^+ (hereafter abbreviated c(H^+)) was performed using pyranine. Notably, for the calibration, it was shown to be important to keep the system as close to the enzymatic reaction setup as possible, with SAM having a strong influence on the calibration curve in general (see Figure S5). By this, the release of protons and therefore successful methylation could be quantified (Figure 3B). The reaction progression curves were shifted to represent the relative formation of H^+ after the start of the reaction (t_0) in order to reflect the enzymatically released protons, since the absolute values are sensitive to small pH variations prior to reaction initiation. While the observed signal can be primarily ascribed to the change of c(H^+) due to the enzymatic reaction, it is not specific to this very process. Instead, it reflects changes in c(H^+) of the entire system. Accordingly, background controls must be run in parallel, for example, by omitting the purified enzyme (Figure 3B).

2.3 | Activity Measurements on MTs With Different Substrate Acceptor Atoms

Having shown that MT activity can generally be monitored *via* a shift in pH during the course of the reaction, the assay set-up was optimised prior to further tests. This was done regarding

the choice of buffer and buffer strength, quenching effects, and calibration procedure (for results and a detailed standard operation procedure, see 'Methods' and Figures S6–S9).

To test the assay's suitability for different application scenarios, methylation activity was determined using the pH assay and compared to results obtained by HPLC (Figure 4). To generate more representative data, three model MTs were used: the *O*-MT *Rn*COMT from *Rattus norvegicus* for the methylation of dopamine (***4***), the *C*-MT *Sr*CouO from *Streptomyces rishiriensis* for the methylation of 2,7-dihydroxy naphthalene (***6***), and the *N*-MT *Sg*PsmC for the methylation of 5-methyl indoline (***2***) used above (Figure 4A). This set of enzymes was chosen in order to include a) MTs with different substrate acceptor atoms, b) MTs targeting different synthetically interesting motifs, and c) MTs which have already been characterized and used in biocatalysis [40–45]. Reactions were prepared in a larger volume, and part of this reaction solution was used for continuous fluorescence measurement to determine released $c(H^+)$. From the remaining reaction volume, samples were taken at dedicated time points, quenched, and analyzed by HPLC for the determination of c(SAH). The corresponding progress curves (Figure 4B) were used to validate the correlation between c(SAH) and $c(H^+)$ (i.e., between HPLC and assay measurements, Figure 4C) and to calculate volumetric enzyme activities (Figure 4D).

Fullest control of pH is difficult to achieve: slight pH differences between calibrations and full reactions, as well as pH fluctuations when combining individual reaction components, cannot be easily prevented. As such, the pH assay is better suited to determine *relative changes* in $c(H^+)$ since the start of the reaction, or—to be more precise,—since the first measurement time point. Because of this, the assay progress curves were shifted so that their datapoint closest to the first HPLC data point (in terms of true reaction time) indicated the same $c(H^+)$ as c(SAH) (see marked positions in Figure 4B).

SAH (HPLC data) and H^+ (assay data) progress curves matched well, especially in the earlier part of the reaction, but did start to diverge after prolonged reaction time and/or higher product concentration (Figure 4B). The deviation differs in strength depending on the reaction system at hand, as is also reflected in differing recovery rates for each enzymatic reaction (Figure 4C). After assay optimization, the recovery rates (RR)—how many H^+ are detected per formed SAH—were 0.96, 0.92, and 0.89 for *Rn*COMT, *Sr*CouO, and *Sg*PsmC, respectively, indicating close to full recovery but also general underrepresentation of c(SAH) when compared to $c(H^+)$.

The underlying reason for varying degrees of deviation between assay and HPLC progress curves is not known. However, two points should be mentioned. Firstly, the different systems are dynamic regarding pH and change over time, irrespectively of the MT-catalyzed reaction, and the progress curves are also measured over time. However, the individual H^+-calibrations are static (i.e., recorded at a single time-point close to and before t_0). As such, the calibrations may reflect the entire system less closely as time progresses, leading to higher deviations after prolonged reaction times (Figure 2B) and to varying degrees depending on the exact system composition. Secondly, the observed variation in recovery rate can also in part be due to experimental error, with a value of approximately 0.92 ± 0.04.

Pearson correlation coefficients were reproducibly >0.99 (Figure 4C), validating the correlation between $c(H^+)$ and c(SAH) formed during the reaction. Enzyme activities determined *via* pH assay were 2%, 7%, and 16% below the HPLC activities, respectively (Figure 4D). When using a two-sided t-test with $\alpha = 5\%$, the null hypothesis could only be rejected for *Sg*PsmC. However, relative changes in enzyme concentration were reflected correctly in the same relative changes in enzyme activity as determined by the assay (see Figure S10). When recovery rates are applied to the assay data, assay results match the HPLC results more closely. This may be important to include in cases where high data fidelity is necessary. Limits of detection (LOD) and of quantification (LOQ) amounted to 12 μM/36 μM for *Rn*COMT, 5 μM/14 μM for *Sr*CouO, and 4 μM/11 μM for *Sg*PsmC based on the close-to-linear range [$c(H^+)$ from 0 μM to 600 μM] of the respective calibration curves (see Figure S15). These values were obtained from calibrations containing 1 mM of the respective methyl acceptor and 1 mM of SAM. For a discussion on the influence of substrate concentration on assay sensitivity, the reader is referred to the section 'Kinetic Measurements With *Rn*COMT'.

To further test the applicability of the assay, *Sg*PsmC substrate acceptance was tested against 5-methyl indoline (***2***) and seven further previously identified [40] indoline substrates (***8*** through ***14***) and compared to HPLC results (Figure 5). Both measurements show similar normalized conversion of the different substrates, ranking them in the same order of substrate acceptance.

The experiment also highlights the importance of individual per-substrate calibrations when working with various substrates with different pK_a values. As the used buffer concentration is kept low (here, 1 mM) to ensure high assay sensitivity, even typical substrate concentrations (here, too, 1 mM) may have a strong effect on the buffering properties of the system, depending on the difference between pK_a(substrate) and pH(system). If this difference is large, the substrate will not substantially contribute to the buffering capacity of the system. If, however, this difference is small, the system's buffering capacity will have been increased, and the assay's sensitivity in turn decreased. This trend can be qualitatively observed when visualizing predicted pK_a values of the tested indolines versus the sensitivity of the individual calibrations (see Figure S12). If, however, a set of substrates shares a similar pK_a, a single calibration can be used without too high an accuracy penalty. Slight deviations from the expected trend can be explained by slightly different initial pH values at the beginning of the calibrations, as well as the qualitative accuracy of the pK_a prediction for substrates of very similar acidity.

The importance of pK_a can also be extended to the reaction product. If both substrate and product have nearly identical pK_a values, a straightforward calibration including only the substrate will suffice (such as for the substrate 2,7-dihydroxy naphthalene (***6***)). If, however, the pK_a values differ, the calibration will introduce larger errors the further the reaction proceeds. For the highest accuracy, the calibration should—with increasing $c(H^+)$—include decreasing substrate and increasing product concentrations to reflect the change of the buffering properties during

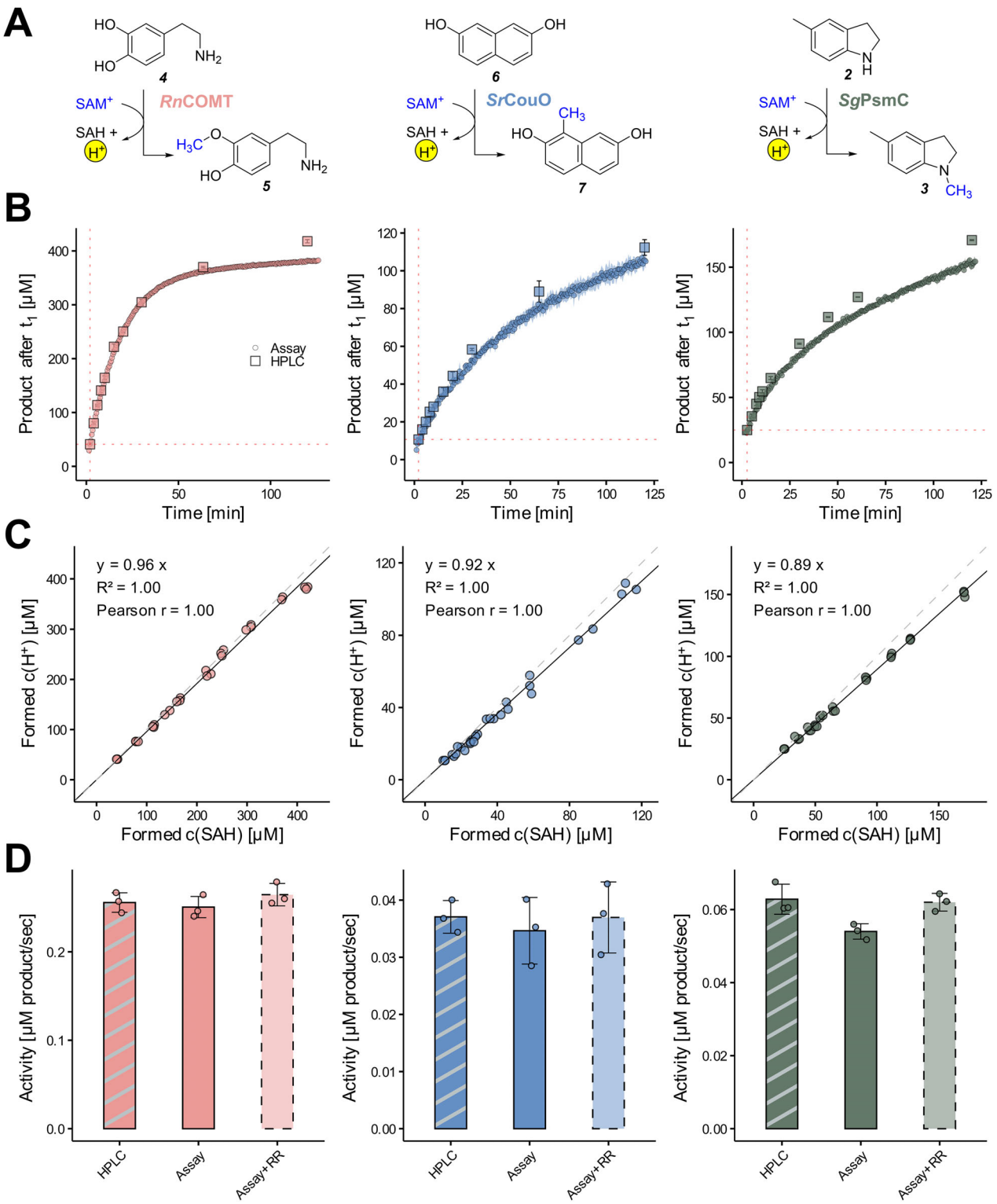

FIGURE 4 | Validation of the suitability of the pH assay to measure MT activity *via* comparison with HPLC data. (A) Catalyzed reactions are used as model systems. (B) Progression curves of each enzyme reaction were recorded both with the pH assay (circles, continuous measurement of $c(H^+)$) and HPLC (squares, discontinuous measurement of c(SAH)). The assay progress curves were shifted so that their datapoint closest to the first HPLC data point (in terms of true reaction time) indicated the same $c(H^+)$ as c(SAH) (indicated by dotted lines). This was done, as the pH assay is better suited to measure relative changes in $c(H^+)$ and not absolute concentrations. (C) Data pairs of $c(H^+)$ and c(SAH) for the closest (regarding true reaction time) data points from the assay and the HPLC progression curves. The slope of the regression curve represents the system-specific recovery rate (RR). *Pearson* correlation coefficients were close to 1. (D) Volumetric enzyme activities as determined by HPLC, by pH assay, and by pH assay corrected by recovery rate ('+RR'). Experimental activities (without correction using the RR) were similar; using a two-sided t-test with $\alpha = 5\%$, the null hypothesis H_0 could only be rejected for *Sg*PsmC. Reaction conditions: 1 mM buffer, 1 mM SAM, 1 mM methyl acceptor, 50 µM pyranine, 10 µM *Sr*CouO / 4.9 µM *Rn*COMT / 5 µM *Sg*PsmC, starting pH 7.5, 25 °C. Experiments were done with $n = 3$ replicates. Errors denote SD.

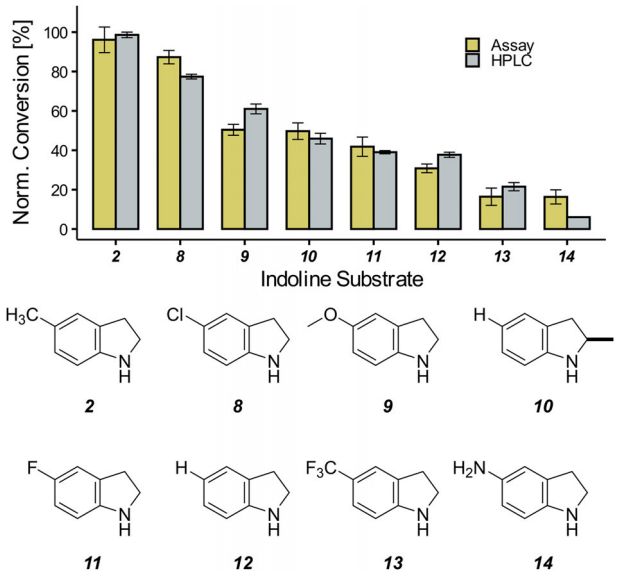

FIGURE 5 | Application of the pH assay for screening various indoline substrates against *Sg*PsmC. Conversion (relative to concentration of used methyl acceptor substrate) after 115 min, normalized to 5-methyl indoline (***2***). 100% normalized conversion in the assay data for substrate (***2***) corresponds to approximately 12% overall conversion (12 μM product), whereas the weaker substrates (***13***) and (***14***) show only about 2% conversion (2 μM product). The same trend regarding substrate acceptance is shown with both HPLC and assay measurement methods. Reaction conditions: 1 mM sodium phosphate buffer, 1 mM SAM, 1 mM indoline substrate, 50 μM pyranine, 1 μM purified *Sg*PsmC; starting pH 7.5, 25 °C.

the reaction course. In general, the closer the calibration reflects the dynamic conditions of the final reaction, the higher the fidelity of the assay data.

2.4 | Kinetic Measurements With *Rn*COMT

As an additional application scenario, steady-state Michaelis-Menten kinetics were recorded for the *O*-methylation of dopamine (***4***) catalyzed by *Rn*COMT with fixed c(SAM). To take the buffering effects of the higher dopamine concentrations into account (see Figure S13; this being necessary to sample reaction velocities close to v_{max}), individual calibrations were recorded for every tested dopamine concentration. Assay sensitivity decreased with increasing dopamine concentration (5% for 1000 μM, 18% for 6000 μM; compared to 0 μM). The Michaelis-Menten equation was fitted to the initial velocities (see Figure S14), leading to $K_M = 219 \pm 20$ μM and $k_{cat} = 0.064 \pm 0.001$ sec^{-1} (Table 1). The same reactions were analysed discontinuously by HPLC measurements, leading to $K_M = 228 \pm 19$ μM and $k_{cat} = 0.074 \pm 0.001$ s^{-1}, indicating general agreement between the two methods.

TABLE 1 | Kinetic parameters obtained by using the pH-shift assay and by HPLC measurements for the *O*-methylation of dopamine (***4***) catalyzed by *Rn*COMT.

Method	K_M [μM]	k_{cat} [sec^{-1}]
pH-shift assay	219 ± 20	0.064 ± 0.001
HPLC	228 ± 19	0.074 ± 0.001

2.5 | Statistical Evaluation for High-Throughput Screenings

When screening large enzyme mutant libraries (e.g., of directed evolution campaigns), most mutants are only tested once: therefore, high fidelity of an assay system to identify beneficial traits (positive hits) is crucial, and an assay's quality for the given application should be assessed before applying it to high-throughput screening (HTS). As preliminary experiments with *Sg*PsmC (see Figure S16) showed that the assay can also be used with CFEs and whole cells, it appeared sensible to also evaluate the assay's applicability in an HTS setting. Thus, the Z'-factor, which takes dynamic range and signal variability into account, was calculated as a statistical measure for intrinsic assay quality based solely on positive and negative control data, using the method described by Zhang et al. [46, 47]. Calculations were performed using the biotechnologically relevant *Rn*COMT [48] and by applying whole-cell catalysts in order to circumvent the need for an additional lysis step.

For this, *Escherichia coli* BL21(DE3) cells were transformed with DNA containing either the native MT gene (positive control) or the backbone plasmid (negative control). Individual colonies were transferred to FlowerPlates for protein production, and cells were harvested and used as whole-cell catalysts. The activity of the enzymatic reaction and negative control was determined using the pH assay, which in turn was used for the determination of the coefficient of variation (CV) as well as the Z'-factor (Figure 6A).

In a first attempt, positive and negative controls were not distinguishable, leading to a calculated Z'-factor of −3.89. At first, this was surprising, as this did not reflect the results of the pre-tests performed with *Sg*PsmC. The only difference—besides the actual choice of catalyst—was that cells had been frozen in the pre-tests prior to their use; the Z'-factor determination for *Rn*COMT was repeated by including an additional freeze-thaw step between cell harvest and assay. Freezing the cells prior to use led to a Z'-factor of 0.70, indicating an excellent assay performance and suitability for HTS in this specific context (Figure 6B). The CV of the positive control was ∼6.2%, which allows identification of mutants with ∼15% increased activity to be identified at a false-positive rate of ∼1%.

Additionally, the Z'-factor was determined for the *N*-MT *Sg*PsmC using fresh, nonfrozen cells. The Z'-factor was −0.32, indicating a poor fit of the assay for HTS screening using this particular system. Despite this, the difference between negative and positive controls was statistically significant (see Figure S17), suggesting that the assay could potentially be employed for screening, albeit with limitations in distinguishing between mutants with marginal decline in performance and the negative control, which can be important to quantify the effect of amino acids crucial for catalysis.

This experiment underlines the importance of evaluating not only the suitability of the assay system for a given application,

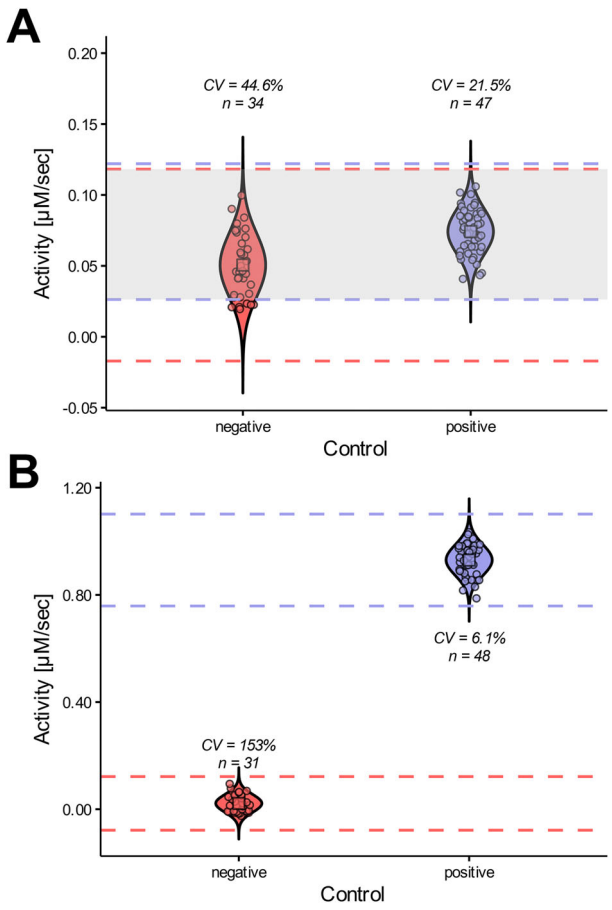

FIGURE 6 | Statistical evaluation of the assay's suitability for HTS based on *Rn*COMT-catalyzed reactions using (A) freshly harvested cells and (B) frozen and thawed cells. The activity of the MT-catalyzed reaction (positive control) was compared to the negative control containing the corresponding empty vector. Mean and individual values are plotted, along with the triple standard deviation (dashed lines), and are color-coded according to the respective datasets. A grey area indicates the overlap of the triple standard deviation of the enzymatic reaction and the negative control. Additionally, the coefficient of variation (CV) was calculated. Reactions, where data could not be fitted reliably for activity calculation (which was the case for some negative control reactions that showed scattering around the baseline), were omitted from the final analysis. Reaction conditions: 1 mM Tris, 3 mM Mg^{2+}; 1 mM dopamine (***4***), 1 mM SAM, 50 µM pyranine, cells at a final OD of 10; starting pH 7.5, 25 °C.

but the entire application workflow (here, including catalyst preparation), prior to initiating an HTS. The performance of a system must be evaluated and validated for each screening to ensure an optimal outcome, particularly when enzyme activity is expected to be very low, and therefore, differences between positive and negative controls are not as pronounced. While the assay is compatible with both purified enzymes and with CFEs—and can as such be considered for HTS applications—whether or not the assay is applicable with freshly harvested, untreated whole-cells must be tested from case to case.

3 | Conclusion

Building on previous work using the fluorophore pyranine for other enzyme classes, an uncoupled, pH-shift-based activity assay was established for the first time for SAM-dependent MTs. The detected increase in $c(H^+)$ during the course of the reaction was shown to directly correlate with the formed c(SAH), and determined activities for a set of three different model enzymes with different methyl acceptor atoms were either close to identical with HPLC control measurements in absolute terms or showed similar differences in relative activity. As a further use case example, different known indoline substrates of the *N*-MT *Sg*PsmC were tested for relative substrate acceptance, and results were in agreement with HPLC readouts. Kinetic measurements are also possible, as was shown for the *O*-methylation of dopamine (***4***) using *Rn*COMT and by comparison with discontinuous measurements by HPLC. As was the case in previous work [32, 33] with other enzyme classes, the pH-shift assay can also be used with CFEs, prompting its use for high-throughput screening. With an additional freeze-thaw step, even whole cells could be used, which were used for the determination of the Z'-factor and intraday CV. These values amounted to 0.70 and ~6.2%, respectively, indicating the assay's potential applicability for HTS.

Due to the assay's nature, fullest control over pH is necessary for the highest sensitivity and data fidelity. As slight pH fluctuations are difficult to circumvent, the assay is best fit to determine relative rather than absolute changes in $c(H^+)$. At the low concentrations of buffering agent needed, enzyme substrates and products can have a strong effect on the system's total buffering capacity and, in turn, on the assay's sensitivity. While substrates (and products) with pK_a values far off the system's pH value will not have a significant effect on the system's buffering capacity, compounds with pK_a values close to the system's pH will. This is more pronounced for higher compound concentrations and more dynamic if the pK_a values of substrate and product pairs differ substantially. However, these points can be taken into account by appropriate calibrations if the experimental conditions demand it or the necessity arises. Since the assay is generally limited to low buffer concentrations in order to achieve high sensitivity [49], it is important to verify that the enzyme is active in this buffer system. If an enzyme requires a higher ionic strength to be active, salts such as NaCl could be added to the buffer, as these will have only a minimal effect on the system's buffering properties.

As addressed throughout this work, different reaction parameters can have varying degrees of effect on the buffering properties of the assay system. Accordingly, a calibration reflecting the chosen reaction setup as closely as possible needs to be recorded prior to measurements of complete enzyme reactions. Deviating from this initial setup may necessitate a new calibration. This may not be the case for parameters with weaker effects (e.g., slight variations in substrate concentration or substitution with a similar substrate of comparable pK_a relative to the system pH). However, for the highest data fidelity—and especially after changing a more impactful condition such as buffer concentrations—a new calibration should be considered. Inherent to the functionality of pH-based assays, pH and temperature profiles of enzymes cannot be measured without added effort: additional pH indicators must be used to extend the assay's currently limited pH window of operation, and further temperature-dependent calibrations would be necessary, respectively. Additionally, the dynamic nature of the system makes careful calibrations and controls essential.

Concluding, the pH-shift assay presented in this work aimed at complementing existing methods: It is (with only a few exceptions) applicable to all SAM-dependent MTs. It is not restricted to purified enzymes, can be used in a high-throughput setting, and allows continuous measurement of MT activity. Furthermore, the used pH-sensitive fluorophore pyranine is well characterized and inexpensive, and—most importantly—no additional enzymes are needed for the detection of MT activity.

4 | Methods

4.1 | Preparation of Solutions

Ideally, all (stock) solutions were prepared in a low-concentration reaction buffer (lc-RB). The lc-RB had a pH value of 7.5 and 1 mM of pH buffering component. Due to limited solubility in aqueous solution, some methyl acceptors had to be prepared as concentrated DMSO stocks (100 mM). The final DMSO concentration in calibrations and reactions never exceeded 2% v/v. A master mix (MM) containing all components (including pyranine, SAM, and methyl acceptor) except for the enzyme was prepared, its pH readjusted once again, and incubated at room-temperature for 30 min prior to starting the assay (see '*Additional Notes*'). Due to the autooxidation of dopamine (***4***), this specific substrate was added to the calibration and reaction mixtures just before measurement. For this, the highest concentrated dopamine substrate stock was prepared just before use, and its pH was adjusted to 7.5 before use. For reactions with CFEs or whole cells, the methyl acceptor was omitted from the MM. However, if the reaction rate was slow, the MM contained all components so that the calibration would reflect the actual reaction conditions more closely. Standard reactions were performed using 1 mM SAM, 1 mM methyl acceptor, and 50 µM pyranine. Reactions with *Rn*COMT also contained 3 mM $MgCl_2$. For *Sg*PsmC and *Sr*CouO, phosphate buffer was used. This buffer was chosen based on previous work [44], as it is commonly used and inexpensive. For *Rn*COMT, Tris buffer was used to hinder precipitation of the cofactor Mg^{2+} [45].

4.2 | Catalyst Preparation

Purified enzymes had to be buffer exchanged with a lc-RB prior to the assay. For this, a small volume concentrator (Vivaspin 500, Sartorius) with an appropriate cut-off was used. Three consecutive concentration-dilution steps (at 12,000 *g* and 4 °C) led to a dilution of the initial storage buffer of at least 1:1,000. For whole cells, frozen or fresh cells (depending on the setup) containing the respective enzyme were washed with 0.9% w/v NaCl, pelleted again, and resuspended in lc-RB. For CFEs, cells were lysed by sonication and cell debris removed by centrifugation.

4.3 | Ratiometric Measurement

Fluorescence was measured using an Infinite M1000 pro plate reader (Tecan, Männedorf, Switzerland) or a FLUOstar Omega plate reader (BMG Labtech, Ortenberg, Germany). For the first device, excitation wavelengths were $\lambda_{ex,1} = 450$ nm and $\lambda_{ex,2} = 405$ nm, and emission was measured at $\lambda_{em} = 510$ nm. For the second device, due to predefined filters, wavelengths were $\lambda_{ex,1} = 485$ nm, $\lambda_{ex,2} = 355$ nm, and $\lambda_{em} = 520$ nm. For analysis, the fluorescence ratio $\frac{F(\lambda_{ex,1}|\lambda_{em})}{F(\lambda_{ex,2}|\lambda_{em})}$ was used, which is further denoted with F450/F405 and F485/F355. Black flat-bottom 96-well plates were used for all reactions.

4.4 | Calibration

For calibration, a dilution series of a reference 1 M HCl solution (Carl Roth, Frankfurt, Germany) was prepared in triplicate. As a dilutant, the respective lc-RB was used. 190 µL of the MM was mixed with 10 µL of the respective HCl solutions in a microtiter plate, and fluorescence was measured. For calibrations intended for reactions with CFE or whole cells, 90 µL of MM and 100 µL of the respective catalyst solution were used instead, to which the 10 µL of the HCl solutions were added. Depending on the range of HCl-concentrations used in the calibration, the following functions (Equations 1 and 2) were used for data fitting.

$$\frac{F\left(\lambda_{ex,1}|\lambda_{em}\right)}{F\left(\lambda_{ex,2}|\lambda_{em}\right)} = m \cdot c\,(HCl) + b \tag{1}$$

$$\frac{F\left(\lambda_{ex,1}|\lambda_{em}\right)}{F\left(\lambda_{ex,2}|\lambda_{em}\right)} = y_0 \cdot A_1 \exp\left(-\frac{c\,(HCl)}{t_1}\right) \tag{2}$$

4.5 | Reactions

Reactions were started by mixing 10 µL of the purified catalysis with 190 µL of MM, and formation of $c(H^+)$ over time was monitored by fluorescence measurement. In case of reactions with CFE and whole cells, the reactions were started by mixing 10 µL of the methyl acceptor, 90 µL of MM, and 100 µL of catalyst solution. Alternatively, if the reaction rate of CFE or whole cell reactions was low, the MM also contained the methyl acceptor. In this case, 10 µL of reaction buffer, 90 µL of MM and 100 µL of catalysts solution were mixed to start the reaction. For CFEs and whole cells, the plate was shaken prior to each measurement.

4.6 | Background Controls

Background-corrected data was obtained by subtracting the respective background controls—run in parallel to all reactions—from the data of full reactions. For reactions with purified enzymes, the enzyme was omitted from the background control. For preliminary reactions with CFE and whole-cells (see Figure S16), the substrate was omitted from the background control. Controls were analysed using separate calibrations to reflect their composition as closely as possible.

4.7 | Standard Analysis

The measured ratio $\frac{F(\lambda_{ex,1}|\lambda_{em})}{F(\lambda_{ex,2}|\lambda_{em})}$ was used to calculate the $c(H^+)$ concentration in the reactions. Reaction progress curves were shifted to represent 'released $c(H^+)$ after t_0', that is, the change of the $c(H^+)$ concentration over the course of the reaction relative to the first data point obtained. Activities were determined by linear regression of the linear part of the progression curve, or by fitting the following function (Equation 3) to the monotonically nondecreasing part of the reaction progress curve covered by the

calibration and then calculating the first derivative of the fitted function at time t = 0 s.

$$c(H^+)(t) = y_0 + A_1 \exp\left(-\frac{t}{t_1}\right) \quad (3)$$

4.8 | Additional Notes

(A) To guarantee that an alkaline pH-shift at the beginning of the reaction (due to mixing of components) or during the reaction (as observed for whole cells and CFEs not containing recombinant MTs) would not lead to the reaction's fluorescence data being outside of the calibrated c(H^+)-range, reactions could be started at a slightly acidified state. For this, reactions were prepared in the presence of 10 µL of one of the respective H^+-calibration solutions. ***(B)*** A slight increase and followed decrease of F450/F405 of MM could be observed when SAM was present (see Figure S11). To counter this, the MM was incubated for 30 min prior to use.

Acknowledgments

We gratefully acknowledge the German Federal Ministry of Education of Research (BMBF, "Modellregion, BioRevierPlus: BioökonomieREVIER Innovationscluster Biotechnologie & Kunststofftechnik-BioTech", grant number 031B1134A), as well as the Heinrich Heine University Düsseldorf and the Forschungszentrum Jülich GmbH for their ongoing support. We thank M. Bickmann for providing us with a first batch of purified *Rn*COMT, Dr. T. Classen for his support in statistical evaluation of data, and Prof. Dr. Fahlke and his group from the Institute of Biological Information Processing (Molekular- und Zellphysiologie IBI-1) for the opportunity to use their fluorescence measuring device.

Open access funding enabled and organized by Projekt DEAL.

Conflicts of Interest

The authors declare no conflicts of interest.

Data Availability Statement

The data that support the findings of this study are available in the supplementary material of this article.

References

1. T. W. Johnson, R. A. Gallego, and M. P. Edwards, "Lipophilic Efficiency as an Important Metric in Drug Design," *Journal of Medicinal Chemistry* 61 (2018): 6401–6420, https://doi.org/10.1021/acs.jmedchem.8b00077.

2. E. Mao and D. W. C. MacMillan, "Late-Stage C(sp3)–H Methylation of Drug Molecules," *Journal of the American Chemical Society* 145 (2023): 2787–2793, https://doi.org/10.1021/jacs.2c13396.

3. H. Schönherr and T. Cernak, "Profound Methyl Effects in Drug Discovery and a Call for New C–H Methylation Reactions," *Angewandte Chemie International Edition* 52 (2013): 12256–12267, https://doi.org/10.1002/anie.201303207.

4. E. Romero, B. S. Jones, B. N. Hogg, et al., "Enzymatic Late-Stage Modifications: Better Late than Never," *Angewandte Chemie International Edition* 60 (2021): 16824–16855, https://doi.org/10.1002/anie.202014931.

5. Y. Chen, "Recent Advances in Methylation: a Guide for Selecting Methylation Reagents," *Chemistry—A European Journal* 25 (2019): 3405–3439, https://doi.org/10.1002/chem.201803642.

6. D. Aynetdinova, M. C. Callens, H. B. Hicks, et al., "Installing the 'Magic Methyl'—C–H Methylation in Synthesis," *Chemical Society Reviews* 50 (2021): 5517–5563, https://doi.org/10.1039/D0CS00973C.

7. M. R. Bennett, S. A. Shepherd, V. A. Cronin, and J. Micklefield, "Recent Advances in Methyltransferase Biocatalysis," *Current Opinion in Chemical Biology* 37 (2017): 97–106, https://doi.org/10.1016/j.cbpa.2017.01.020.

8. D. A. Amariei, J. Tenhaef, T. Classen, et al., "Directed Evolution of C-methyltransferase PsmD for Enantioselective Pyrroloindole Derivative Production," *Catalysis Science & Technology* 14 (2024): 6298–6306, https://doi.org/10.1039/D4CY00657G.

9. J. Zhang and Y. G. Zheng, "SAM/SAH Analogs as Versatile Tools for SAM-Dependent Methyltransferases," *ACS Chemical Biology* 11 (2016): 583–597, https://doi.org/10.1021/acschembio.5b00812.

10. C. Liao and F. P. Seebeck, "S-adenosylhomocysteine as a Methyl Transfer Catalyst in Biocatalytic Methylation Reactions," *Nature Catalysis* 2 (2019): 696–701, https://doi.org/10.1038/s41929-019-0300-0.

11. S. Mordhorst, J. Siegrist, M. Müller, M. Richter, and J. N. Andexer, "Catalytic Alkylation Using a Cyclic S -Adenosylmethionine Regeneration System," *Angewandte Chemie International Edition* 56 (2017): 4037–4041, https://doi.org/10.1002/anie.201611038.

12. K. H. Schülke, F. Ospina, K. Hörnschemeyer, S. Gergel, and S. C. Hammer, "Substrate Profiling of Anion Methyltransferases for Promiscuous Synthesis of S-Adenosylmethionine Analogs from Haloalkanes," *ChemBioChem* 23 (2022): e202100632, https://doi.org/10.1002/cbic.202100632.

13. M. E. K. Salyan, D. L. Pedicord, L. Bergeron, et al., "A General Liquid Chromatography/Mass Spectroscopy-based Assay for Detection and Quantitation of Methyltransferase Activity," *Analytical Biochemistry* 349 (2006): 112–117, https://doi.org/10.1016/j.ab.2005.10.040.

14. J. M. Hevel and O. M. Price, "Rapid and Direct Measurement of Methyltransferase Activity in About 30 Min," *Methods (San Diego, Calif)* 175 (2020): 3–9, https://doi.org/10.1016/j.ymeth.2019.10.002.

15. D. A. Amariei, M. Haase, M. K. T. Klischan, M. Wäscher, and J. Pietruszka, "High-Throughput Colorimetric Detection and Quantification of Indoles and Pyrroloindoles for Enzymatic Activity Determination," *Chemical Catalysis* 16 (2024): e202400052, https://doi.org/10.1002/cctc.202400052.

16. Q. Tang, C. W. Grathwol, A. S. Aslan-Üzel, et al., "Directed Evolution of a Halide Methyltransferase Enables Biocatalytic Synthesis of Diverse SAM Analogs," *Angewandte Chemie International Edition* 60 (2021): 1524–1527, https://doi.org/10.1002/anie.202013871.

17. H. Simon-Baram, S. Roth, C. Niedermayer, et al., "A High-Throughput Continuous Spectroscopic Assay to Measure the Activity of Natural Product Methyltransferases," *ChemBioChem* 23 (2022): e202200162, https://doi.org/10.1002/cbic.202200162.

18. S. Duchin, Z. Vershinin, D. Levy, and A. Aharoni, "A Continuous Kinetic Assay for Protein and DNA Methyltransferase Enzymatic Activities," *Epigenetics & Chromatin* 8 (2015): 56, https://doi.org/10.1186/s13072-015-0048-y.

19. L. L. Kailing, D. Bertinetti, F. W. Herberg, and I. V. Pavlidis, "A Coupled Photometric Assay for Characterization of *S*-adenosyl-l-homocysteine Hydrolases in the Physiological Hydrolytic Direction," *New Biotechnology* 39 (2017): 11–17, https://doi.org/10.1016/j.nbt.2017.04.005.

20. C. L. Hendricks, J. R. Ross, E. Pichersky, J. P. Noel, and Z. S. Zhou, "An Enzyme-coupled Colorimetric Assay for *S*-adenosylmethionine-dependent Methyltransferases," *Analytical Biochemistry* 326 (2004): 100–105, https://doi.org/10.1016/j.ab.2003.11.014.

21. D. Schulz and A. Rentmeister, "An Enzyme-coupled High-throughput Assay for Screening RNA Methyltransferase Activity in E. Coli Cell Lysate," *RNA Biology* 9 (2012): 577–586, https://doi.org/10.4161/rna.19818.

22. Y. Tan and R. M. Hoffman, "A Highly Sensitive Single-enzyme Homocysteine Assay," *Nature Protocols* 3 (2008): 1388–1394, https://doi.org/10.1038/nprot.2008.117.

23. M. J. Menke, P. Schneider, C. P. S. Badenhorst, et al., "A Universal, Continuous Assay for SAM-Dependent Methyltransferases," *Angewandte Chemie International Edition* 62 (2023): e202313912, https://doi.org/10.1002/anie.202313912.

24. M. K. Akhtar, D. Vijay, S. Umbreen, et al., "Hydrogen Peroxide-Based Fluorometric Assay for Real-Time Monitoring of SAM-Dependent Methyltransferases," *Frontiers in Bioengineering and Biotechnology* 6 (2018), https://doi.org/10.3389/fbioe.2018.00146.

25. K. M. Dorgan, W. L. Wooderchak, D. P. Wynn, et al., "An Enzyme-coupled Continuous Spectrophotometric Assay for *S*-adenosylmethionine-dependent Methyltransferases," *Analytical Biochemistry* 350 (2006): 249–255, https://doi.org/10.1016/j.ab.2006.01.004.

26. R. T. Borchardt and Y. S. Wu, "Potential Inhibitors of S-adenosylmethionine-dependent Methyltransferases. 1. Modification of the Amino Acid Portion of S-adenosylhomocysteine," *Journal of Medicinal Chemistry* 17 (1974): 862–868, https://doi.org/10.1021/jm00254a016.

27. K. Hsiao, H. Zegzouti, and S. A. Goueli, "Methyltransferase-Glo: a Universal, Bioluminescent and Homogenous Assay for Monitoring all Classes of Methyltransferases," *Epigenomics* 8 (2016): 321–339, https://doi.org/10.2217/epi.15.113.

28. F. Morís-Varas, A. Shah, J. Aikens, N. P. Nadkarni, J. D. Rozzell, and D. C. Demirjian, "Visualization of Enzyme-catalyzed Reactions Using pH Indicators: Rapid Screening of Hydrolase Libraries and Estimation of the Enantioselectivity," *Bioorganic & Medicinal Chemistry* 7 (1999): 2183–2188, https://doi.org/10.1016/S0968-0896(99)00149-2.

29. P. Holloway, J. T. Trevors, and H. Lee, "A Colorimetric Assay for Detecting Haloalkane Dehalogenase Activity," *Journal of Microbiological Methods* 32 (1998): 31–36, https://doi.org/10.1016/S0167-7012(98)00008-6.

30. K. Yu, S. Hu, J. Huang, and L.-H. Mei, "A High-throughput Colorimetric Assay to Measure the Activity of Glutamate Decarboxylase," *Enzyme and Microbial Technology* 49 (2011): 272–276, https://doi.org/10.1016/j.enzmictec.2011.06.007.

31. M. F. Paye, H. B. Rose, J. M. Robbins, D. A. Yunda, S. Cho, and A. S. Bommarius, "A High-throughput pH-based Colorimetric Assay: Application Focus on Alpha/Beta Hydrolases," *Analytical Biochemistry* 549 (2018): 80–90, https://doi.org/10.1016/j.ab.2018.03.009.

32. A. V. Sunder, M.-L. Reif, and W.-D. Fessner, "Fluorescence-based pH-shift Assay with Wide Application Scope for High-throughput Determination of Enzymatic Activity in Enzyme Mining and Engineering," *Catalysis Science & Technology* 14 (2024): 5375–5384, https://doi.org/10.1039/D4CY00566J.

33. S. Nevolova, E. Manaskova, S. Mazurenko, J. Damborsky, and Z. Prokop, "Development of Fluorescent Assay for Monitoring of Dehalogenase Activity," *Biotechnology Journal* 14 (2019): 1800144, https://doi.org/10.1002/biot.201800144.

34. H. Mu, L. Ye, and B. Wang, "Detailed Resume of S-methyltransferases: Categories, Structures, Biological Functions and Research Advancements in Related Pathophysiology and Pharmacotherapy," *Biochemical Pharmacology* 226 (2024): 116361, https://doi.org/10.1016/j.bcp.2024.116361.

35. R. Nandi and N. Amdursky, "The Dual Use of the Pyranine (HPTS) Fluorescent Probe: a Ground-State pH Indicator and an Excited-State Proton Transfer Probe," *Accounts of Chemical Research* 55 (2022): 2728–2739, https://doi.org/10.1021/acs.accounts.2c00458.

36. G. Panzarasa, A. Osypova, C. Toncelli, et al., "The Pyranine-benzalkonium Ion Pair: a Promising Fluorescent System for the Ratiometric Detection of Wound pH," *Sensors and Actuators B: Chemical* 249 (2017): 156–160, https://doi.org/10.1016/j.snb.2017.04.045.

37. Y. Hiruta, N. Yoshizawa, D. Citterio, and K. Suzuki, "Highly Durable Double Sol–Gel Layer Ratiometric Fluorescent pH Optode Based on the Combination of Two Types of Quantum Dots and Absorbing pH Indicators," *Analytical Chemistry* 84 (2012): 10650–10656, https://doi.org/10.1021/ac302178z.

38. A. Chang, L. Jeske, S. Ulbrich, et al., "BRENDA, the ELIXIR Core Data Resource in 2021: New Developments and Updates," *Nucleic Acids Research* 49 (2021): D498–D508, https://doi.org/10.1093/nar/gkaa1025.

39. J. Liu, T. Ng, Z. Rui, O. Ad, and W. Zhang, "Unusual Acetylation-Dependent Reaction Cascade in the Biosynthesis of the Pyrroloindole Drug Physostigmine," *Angewandte Chemie International Edition* 53 (2014): 136–139, https://doi.org/10.1002/anie.201308069.

40. B. P. Chapple, L. Nitz, P. Schneider, et al., "Characterisation of the N -Methyltransferase Sg PsmC: Application in the Kinetic Resolution of Pyrroloindolines," *Angewandte Chemie International Edition* 65 (2026): e15459, https://doi.org/10.1002/anie.202515459.

41. H.-S. Kim, J.-A. Choi, B.-Y. Kim, et al., "Engineered Corynebacterium Glutamicum as the Platform for the Production of Aromatic Aldehydes," *Frontiers in Bioengineering and Biotechnology* 10 (2022), https://doi.org/10.3389/fbioe.2022.880277.

42. B. J. C. Law, M. R. Bennett, M. L. Thompson, et al., "Effects of Active-Site Modification and Quaternary Structure on the Regioselectivity of Catechol-O-Methyltransferase," *Angewandte Chemie* 128 (2016): 2733–2737, https://doi.org/10.1002/anie.201508287.

43. T. Pavkov-Keller, K. Steiner, M. Faber, et al., "Crystal Structure and Catalytic Mechanism of CouO, a Versatile C-Methyltransferase from Streptomyces Rishiriensis," *PLoS One* 12 (2017): e0171056, https://doi.org/10.1371/journal.pone.0171056.

44. H. Stecher, M. Tengg, B. J. Ueberbacher, et al., "Biocatalytic Friedel–Crafts Alkylation Using Non-Natural Cofactors," *Angewandte Chemie International Edition* 48 (2009): 9546–9548, https://doi.org/10.1002/anie.200905095.

45. J. Vidgren, L. A. Svensson, and A. Liljas, "Crystal Structure of Catechol O-methyltransferase," *Nature* 368 (1994): 354–358, https://doi.org/10.1038/368354a0.

46. J.-H. Zhang, T. D. Y. Chung, and K. R. Oldenburg, "A Simple Statistical Parameter for Use in Evaluation and Validation of High Throughput Screening Assays," *SLAS Discovery* 4 (1999): 67–73, https://doi.org/10.1177/108705719900400206.

47. O. Salazar and L. Sun in *Directed Enzyme Evolution: Screening and Selection Methods*, (eds.: F.H. Arnold and G. Georgio. (Humana Press, 2003): 85–97, https://doi.org/10.1385/1592593968.

48. K. Li and J. W. Frost, "Synthesis of Vanillin from Glucose," *Journal of the American Chemical Society* 120 (1998): 10545–10546, https://doi.org/10.1021/ja9817747.

49. L. E. Janes, A. C. Löwendahl, and R. J. Kazlauskas, "Quantitative Screening of Hydrolase Libraries Using pH Indicators: Identifying Active and Enantioselective Hydrolases," *Chemistry—A European Journal* 4 (1998): 2324–2331, https://doi.org/10.1002/(SICI)1521-3765(19981102)4:11%3C2324::AID-CHEM2324%3E3.0.CO;2-I.

Supporting Information

Additional supporting information can be found online in the Supporting Information section.

The authors have cited additional references within the Supporting Information.

Supporting File: cctc70581-sup-0001-SuppMat.pdf.